URTeC: 4042958

Geochemically-driven Petrophysical Transformations in Caney Shale and their Impact on Reservoir Productivity

Gabriel Awejori[*1], Wenming Dong[2], Christine Doughty[2] and Mileva Radonjic[1,3]

[1]Geomimicry and Barrier Materials Labs, School of Chemical Engineering, Oklahoma State University, Stillwater, OK 74078, USA

[2]Energy Geosciences Division, Lawrence Berkeley National Laboratory, 1 Cyclotron Road, Berkeley, CA 94720, USA

[3]Boone Pickens School of Geology, Oklahoma State University, Stillwater, OK 74078, USA

Abstract

In this paper, we report research findings on geochemical rock-fluid interactions between Caney Shale samples and completion fluids used for hydraulic fracturing, and how these reactions impact reservoir productivity. Hydraulic fracturing of shales triggers a series of dissolution, precipitation reactions and ion exchange in clays, resulting in the alteration of reservoir petrophysical properties, including conductivity of hydraulic fractures. These reactions are largely dependent on the chemical compositions of the fluids and reservoir rock mineralogy.

In this study, static batch reactor experiments are employed where rock-slabs and rock-powders are reacted with produced brine. The reactions are conducted at temperature of 95^{o}C in sealed pyrex reaction bottles, with sampling at the beginning and after four 4 weeks. There was no external pressurization applied to the reaction bottles. Mineralogical characterization of Caney Shale samples before and after reaction are conducted using x-ray diffraction (XRD) whilst microstructural and elemental analyses are studied using scanning-electron microscopy (SEM) and energy dispersive spectroscopy (EDS) respectively.

The results show changes in the elemental and mineralogical composition of rock-slabs and powdered rock samples respectively, therefore confirming geochemical reactions occurred during the experimental period. XRD measurements of rock-powders before and after reaction show decreases of pyrite, feldspar, and carbonate contents whiles quartz and illite contents either remained the same or increased. In terms of elemental compositions on the surface of rock-slabs, there is significant change to the pyrite elemental composition due to oxidation-induced dissolution. Precipitation of new minerals and amorphous entities is also observed on the surface of rock-slabs. These results reveal that geochemical reactions following hydraulic fracturing persist in the long-term. The breakdown of pyrite by dissolved oxygen or breakdown of oxidants can lead to higher localized acidity which can dissolve more minerals resulting in higher

elemental ion concentrations in the system. The dissolved elemental ions subsequently form new mineral precipitates which can occlude hydrocarbon flow-paths and lead to loss of permeability and productivity decline from a reservoir.

This study provides an appreciation of the post-fracturing geochemical rock-fluid reactions and the impact of these reactions on long-term permeability of shale reservoirs. The study also shows the initiation of geochemical reactions during shut-in where hydraulic fracturing fluids are imbibed by the reservoir rock. This study can therefore serve as a basis from which composition of hydraulic fracturing fluids are fine-tuned to mitigate adverse geochemical rock-fluid reactions in the subsurface, post-hydraulic fracturing.

1.0 Introduction

The challenge with horizontal drilling and hydraulic fracturing of tight unconventional reservoirs is that the increased permeability generated from the hydraulically stimulated fracture networks can be short-lived. The variable decay of the fracture networks contributes to the highly variable well performance reported across fields and between proximal wells and inherently low recovery factors from these reservoirs which stands at approximately 10% (Mukhina et al., 2021).The closure of hydraulically stimulated fractures is the result of adverse geochemical reactions and high confining pressures in the subsurface. Whilst some researchers place emphasis on predominance of mechanically-driven fracture closure processes (Allen et al., 2 022; Benge et al., 2021; Katende et al., 2023; Wood and Milne, 2011), others are proponents of chemically-driven fracture closure (Awejori et al., 2022; Esteves et al., 2022; Liu et al., 2018; Marcon et al., 2017; Olabode and Radonjic, 2017).

Drilling and hydraulic fracturing are mostly undertaken using water-based drilling muds and fracturing fluids respectively (Aftab et al., 2020; Ahmed et al., 2021; Maiti et al., 2021; Yalman et al., 2022). During these operations, the water-based completion fluids lost to the stimulated reservoir can trigger geochemical reactions that cause formation damage. In the case of hydraulic fracturing, completion fluids injected into the formation are imbibed into the fracture walls and then into the matrix pore system of the formation. These fluids can be incompatible with the formation water and petroleum, which creates disequilibrium conditions that can cause a series of dissolution and precipitation reactions. These reactions can cause the blockage of nano-pores linking the fracture and rock matrix, thus substantially impairing the permeability of the reservoir (Almulhim et al., 2014; Chakraborty et al., 2017; Li et al., 2020; Liu et al., 2018; Zhou et al., 2016). It is therefore imperative to assess injected fluid compatibility with subsurface fluids in the context of the driving forces of these reactions to minimize adverse impacts and enhance the favorable impacts.

This study examines the contribution of geochemical rock-fluid interactions initiated by completion fluids to fracture closure in hydraulically fractured shale reservoirs. Understanding these processes will help to mitigate long-term permeability losses associated with shale reservoirs and improve their ultimate recovery .

1.1 Shale Mineralogy and Post-Fracturing Reactions

In the early days of petroleum exploration and exploitation, shales were identified as source rocks in which hydrocarbons were generated and as seal rocks which prevented hydrocarbon migration and trapped them within a reservoir unit (Dewhurst et al., 2002; Downey, 1984; Luning et al., 2005). The interest in shale was therefore in context of having enough organic matter and obtaining the required level of thermal maturity to generate economically significant volumes of petroleum as well as their ability to prevent upward migration of petroleum fluids due to their low permeability and high capillary entry pressures. However, the advent of unconventional hydrocarbon exploitation and geological carbon storage has changed the way in which shales are viewed. Though organic-rich shales generate and expel hydrocarbons found in conventional reservoirs, they also provide substantial storage for economic accumulation of hydrocarbons (Feng et al., 2021). Recently, depleted shale reservoirs have been evaluated as potential sinks for carbon dioxide captured from industrial plants and other sources (Khosrokhavar et al., 2014; Tayari et al., 2015). In this regard, shale plays around the world have become key economic resources.

Shales are the most common type of sedimentary rock and generally include rocks with argillicious grain sizes, such as mudstone, and claystone. The mineralogical composition of shales varies but they are generally made up of quartz, feldspar, clay minerals, carbonate, and organic matter compositions. Shaw and Weaver, (1965) documented the mineralogical composition of 300 shale samples showing a wide range of compositions with average values as follows: quartz – 30.8%, feldspar – 4.5%, carbonate – 3.6%, clay minerals – 60.9%, iron oxide - <0.5%. The mineralogy of some producing shales however varies significantly from these average compositions. The mineralogical compositions of shales play a significant role in their properties and how they respond to chemical and mechanical stresses. In general, shales with higher clay mineral content tend to be chemically reactive and exhibit ductile properties compared to shales with higher quartz compositions.

In relation to exploitation of hydrocarbons from shales with ultra-low permeability, horizontal drilling and hydraulic fracturing remain the most viable techniques (Soeder, 2018). The chemical response of shale to hydraulic fracturing is known to directly impact the petrophysical properties of the rock over long periods. Chemical reactions between shales and fracturing fluids lead to dissolution and precipitation reactions which alter the petrophysical properties of the formation (Harrison et al., 2017; Xiong et al., 2022). During dissolution of minerals, the porosity of the formation increases, however the release of ions into the system sets off a series of chemical reactions which triggers precipitation of new minerals. The new minerals precipitated during fracturing nucleate and grow within pores and the fracture system of the shales which significantly decreases the permeability of the reservoir.

2.0 Materials and Methodology

This study is aimed at understanding the impact of post-fracturing rock-fluid reactions on mineralogy, microstructure, and petrophysical properties of the fracture face. The study also seeks to draw a link between rock-fluid reactions for rock-powder samples and rock-slab samples to understand the kinetics associated with each sample type. Experiments are therefore designed to recreate as closely as possible reservoir conditions in the subsurface of typical unconventional shale reservoirs.

2.1 Materials

Samples used for batch reactor experiments are mainly shale rocks and produced brines from the Caney Shale. The rock samples include polished rock-slabs and powdered samples. Rock-slab samples are extracted in two orientations: samples cored parallel to the bedding plane (horizontal samples) and samples cored normal to the bedding plane (vertical samples). These samples are extracted at selected depths from core retrieved from a vertical well in the Caney Shale. These depths represent seal and reservoir zones of the shale. These classifications are based on definitions by industry operator in the well location (Awejori et al., 2022). For the purposes of this study, the samples are classified as ductile and reservoir samples. The fluid used in the experiments is produced brine from a well producing in the Caney Shale. The cation composition of the produced brine based on inductively coupled plasma mass spectroscopy (ICPMS) analysis is presented in **Table 1**.

Table 1: Major element concentrations in produced brine used for experiments.

Na (ppm)	Mg (ppm)	Al (ppm)	Si (ppm)	P (ppm)	K (ppm)	Ca (ppm)	Fe (ppm)	Sr (ppm)	Ba (ppm)
16445.09	77.47	0.19	33.75	0.12	71.79	554.91	5.79	79.77	17.51

2.2 Sample Preparation

Sample preparation for rock-slabs is significantly different from that used for powdered rock samples. Both sample preparations are designed to minimize contamination. In this regard, sample preparation is undertaken systematically and presented in the following:

2.2.1 Polished Rock-Slab

- Core plugs are drilled from depths to be sampled at defined orientations. These are 2inch x 1inch (length and diameter respectively) in size.
- Rock-slab of half inch thickness is cut from the core plug with the fresh-cut face noted.
- The freshly cut face of the rock-slab is polished using alcohol-based polishing lubricants to ensure minimal reaction of shale minerals with polishing fluids.
- The polishing of each sample involves five levels of polishing surfaces – 400 grit paper, 600 grit paper, gold label polishing surface, white label polishing surface and black label polishing surface.
- The polishing fluids used include 6µm diamond polish, 1µm diamond polish, and silica gel, which are respectively used on the gold, white, and black polishing surfaces.
- The main lubricant employed for polishing is purple lube which is applied in all polishing stages except on the black label polishing surface where only silica gel is used.
- The amount of time during each stage of the polishing process averages 5 minutes.
- Polished rock-slabs for vertical and horizontal reservoir samples are shown in Fig. 1a and Fig. 1b respectively.

2.2.2 Powdered Rock Samples (Rock Powders)

- The core plugs drilled out of the target depths are first crushed into smaller chippings with a hammer.
- These chippings are ground to powder using a Spex ball mill.
- The samples are further comminated using McCrone microniser to reduce the particle size to size passing 400 mesh size (100 µm).

2.3 Experimental Setup

Static batch reactor experiment is one of the most established experimental methods used in the study of rock-fluid reactions. This method is based on the premise that, following hydraulic fracturing, wells are shut in for an average of three weeks before production is resumed. In this period, the injected completion fluid encounters and reacts with formation fluids and rock.

In this set of static batch experiments, the mass of polished rock-slab samples is measured and recorded. The mass of produced brine, approximately fifteen (15) times the mass of the rock-slab is also measured, and the rock-slab placed in fluid giving a mass ratio of 1g of bulk rock to 15g of produced brine. In terms of powdered rock samples, 2-grams of rock sample is mixed with 200mL of produced brine to give an initial rock powder to fluid ratio of 1g to 100mL. The samples are mixed in pyrex bottles and vigorously agitated to ensure thorough mixing. The pyrex bottles are subsequently put in an oven preset to 95^{o}C (203^{o}F). The samples are allowed to react for four (4) weeks.

2.4 Sampling

Sampling is undertaken at the end of experiment for both types of experiments. Description of the sampling process in both types of experiments is presented below.

For batch samples in which polished rock-slabs are reacted with fluids, the samples are removed from the oven and the rock sample is removed from the produced brine. The rock-slab is rinsed with isopropanol for approximately 30 seconds before it is allowed to dry and placed in container. This is done to ensure the halting of further reaction on the sample. Post-experimental analyses are subsequently undertaken. The brine is allowed to cool before sampling with a syringe and filtered through 0.22µm filter. This reacted brine is stored in a refrigerator awaiting ICPMS elemental analysis.

For rock powdered samples, the reaction bottles holding rock and fluid mixture are removed from the oven and allowed to cool for about 10 minutes. The fluid is then decanted from the bottle into a beaker leaving the rock powder and small amount of fluid in the pyrex reaction bottle. The fluid is sampled with syringe and filtered with 0.22µm filter by attaching the filter to the base of the syringe. The fluid is stored in a refrigerator awaiting ICPMS elemental analysis. The fluid left in the reaction bottle with rock powders is removed from the rock powder through evaporation. The evaporation is achieved by putting the opened sample bottles in an oven and increasing the temperature of the oven from 30^{o}C to 60^{o}C (86^{o}F to 140^{o}F) over a period of 2 hours and leaving it steady for the next 24 hours. During this period, the vent of the oven is opened to allow water vapor to escape. The rock powders are subsequently retrieved from the pyrex reaction bottles and stored in glass vials.

During sampling, the pH of the fluids is measured and compared with initial fluid pH at the beginning of the experiments. These are presented in Table 2.

Table 2: pH measurements of fluids at beginning and end of experiment.

Sample	Ductile Horizontal	Ductile Vertical	Reservoir Horizontal	Reservoir Vertical	Ductile Powder	Reservoir Powder
Day 0	7.69	7.68	7.68	7.71	7.63	7.63
Day 28	7.67	7.73	7.43	7.35	8.20	7.17

2.5 Analytical Methods

Rock samples are analyzed before and after experiment to delineate the changes that occurred over the reaction period. It is worth noting that changes in samples are subtle, especially in the polished rock-slabs where reaction is expected to be slow. Polished and powdered samples are therefore analyzed using different techniques to ensure identification of all changes that occurred. The following is a summary of analytical techniques and conditions which are employed.

Scanning electron microscopy is used to study the microstructural configuration of the polished rock-slabs. This is achieved with Scios scanning electron microscope in backscatter electron mode with a working distance of approximately 7µm. For the pre-reaction sample, no coating is applied. The voltage and current settings are 5kV and 3.2nA respectively and micrographs are acquired at various magnifications (x100, x200, x500, x1000 and x2000). For the post-reaction sample, about 1nm of iridium coating is applied. The voltage and current settings include 10kV and 3.2nA respectively and micrographs are acquired at various magnifications (x100, x200, x500, x1000 and x2000). The different magnifications allowed perceiving of the microstructural configuration at different scales. Micrographs and maps of magnification 500x are used in this paper to ensure consistency with elemental maps which are all acquired at this magnification. The microstructural studies are complemented by elemental mapping using the Pathfinder EDS X-ray microanalysis software attached to the Scios scanning electron microscope. The EDS analysis is undertaken for both freshly polished rock-slabs and reacted rock-slabs.

The mineralogical compositions of the powdered rock samples are evaluated using the Bruker D8 Advanced X-Ray Diffractometer with a Lynxeye detector. Scanning angles ranged from 5 to 80 degrees 2-theta angle with 0.01-degree step size and a dwell time of 0.5 seconds. The voltage and current setting for XRD analyses are 40kV and 40mA respectively. Semi-quantitative analyses are subsequently undertaken on the samples using BRUKER's Diffrac.suite eva software. Three measurements are undertaken for each sample before and after experiments and an average value calculated.

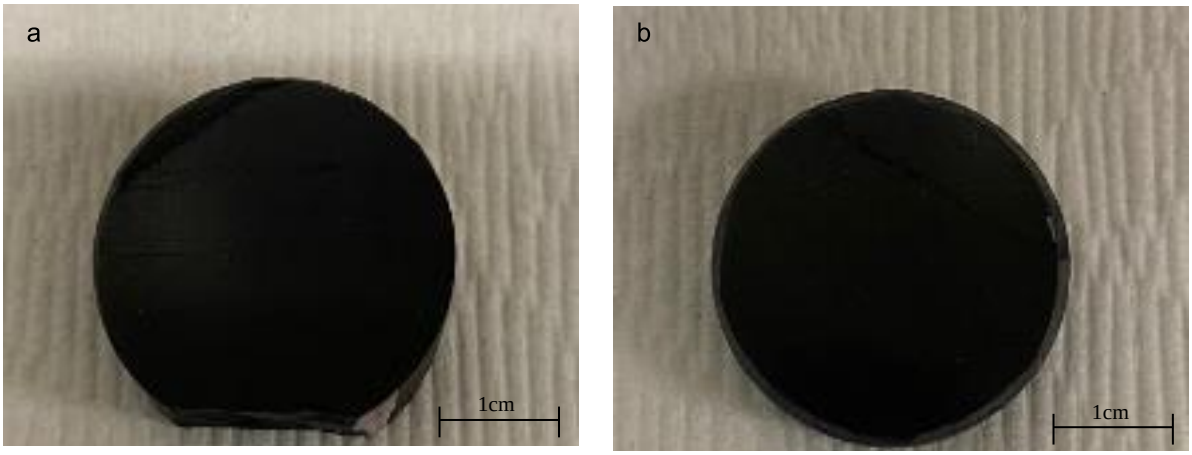

Reservoir Horizontal Sample **Reservoir Vertical Sample**

Fig. 1: Photograph of polished samples a). horizontal samples of reservoir 3 (R3) rocks prepared for pre-reaction SEM and EDS data acquisition b). vertical samples of reservoir 3 (R3) rocks prepared for pre-reaction SEM and EDS data acquisition.

3.0 Results

3.1 Mineralogy of Powdered Samples

The initial mineralogical composition of the samples is consistent with mineralogy estimated in various studies on the Caney Shale (Awejori et al., 2021; Wang et al., 2021). XRD analyses showed the samples to be predominantly quartz, feldspar, carbonates and illite-smectite with minor amounts of pyrite as shown on Fig. 2. The most common carbonates identified in the samples are calcite and dolomite whilst the most common feldspar is plagioclase. Following reaction with produced brines, the mineralogical composition of the powdered rock underwent transformations, albeit not pronounced as in reaction with field-fracturing fluids recorded in Awejori et al., (2022). These changes are however significant compared to changes observed from SEM and EDS micro-analysis on rock-slab samples.

The key mineralogical changes observed from XRD analyses include reduction of feldspar and pyrite contents with corresponding increase in quartz, illite-smectite and carbonates. It is inferred that reactions cause dissolution of pyrite and feldspar with corresponding precipitation of carbonates due to initially high Ca ion concentrations in produced brines. Though increased weight percent of quartz and illite-smectite may be attributable to the renormalization of the weight percents of minerals following the dissolution of pyrite and feldspar, illitization of feldspar cannot be ruled out as responsible for increased illite-smectite content. The trends observed in pH of fluids, where the pH increased or decreased marginally over the reaction period is consistent with the non-dissolution of carbonates in this reaction. The buffering effect of carbonate dissolution is therefore not conspicuous relative to reactions where the starting pH is acidic. To corroborate the foregoing trend, carbonate dissolution is relatively slow compared to reactions where initial fluid pH is acidic and rock-fluid ratio is high (Fu et al., 2015; Morse and Arvidson, 2002). The complete dissolution of pyrite may be attributed to high oxygen content in produced brines. Though samples were exposed to oxygen during the drying process, it is believed that this reaction is minimal and could not be responsible for complete dissolution of pyrite. In essence, reactions in this experiment replicate long-term rock-fluid interactions where initial acid spear in fracturing fluid has been depleted and fracturing fluid has completely mixed with formation fluid to form a hybrid fluid (produced brine).

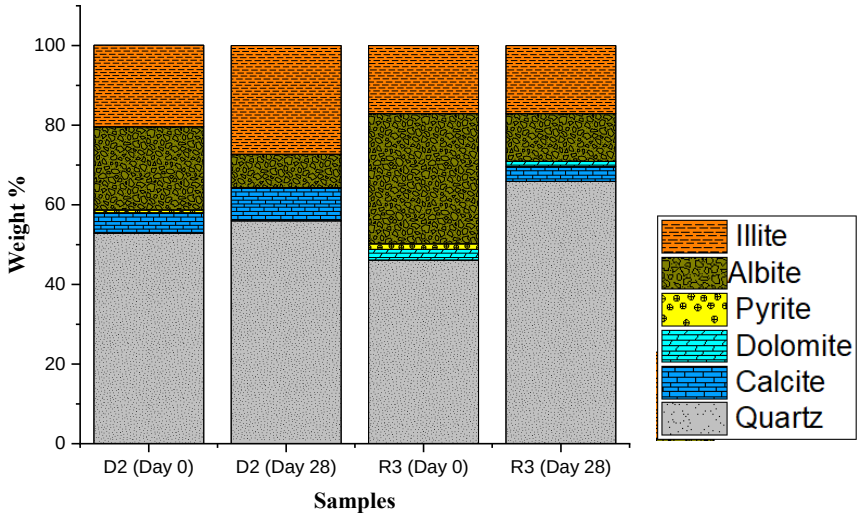

Fig. 2: Mineralogical compositions of rock-powders before and after interaction with produced brines for 28-days. D2 (Day 0) represents mineralogy of ductile 2 sample before reaction, D2 (Day 28) represents mineralogy of ductile 2 sample after 28-days reaction, R3 (Day 0) represents mineralogy of reservoir 3 sample before reaction, R3 (Day 28) represents mineralogy of reservoir 3 sample after 28-days reaction.

3.2 Scanning Electron Microscopy and Energy Dispersive Spectroscopy on Rock-Slab Samples

The results presented in this section include SEM micrographs showing the mineralogy and microstructure of samples whilst EDS microanalysis shows the elemental compositions of the samples. These are acquired before and after the static batch reactor experiments. From SEM and EDS analyses, the samples are largely made up of quartz, carbonates, felspars, and pyrite embedded in a matrix of clay minerals, which is predominantly illite-smectite.

The following presents a summary of SEM and EDS analyses on samples before reaction and after reaction with produced brine which provides an understanding of transformations that are occasioned by reactions between rocks and fluids.

3.2.1 Ductile Horizontal Sample

The direction of coring of this sample is normal to the main core/wellbore axis (i.e., parallel to the bedding plane). The microstructural configuration of the sample before reaction shows grains of quartz, carbonates, framboidal pyrite and disseminated pyrite encapsulated in matrix of clay minerals. The grain sizes common in this sample range from 5µm to 30µm with an average grain size of less than 20µm. The common contact in the sample is grain-matrix contact. Preferred orientation of minerals is observed in this sample as shown in Fig. 3a. In terms of EDS microanalysis, the elemental concentrations by weight % indicates the presence of Si, Al, Mg, Fe, S, and Ca (Fig. 4a,b). These elements are synonymous with minerals like quartz, illite-smectite, dolomite, pyrite, plagioclase, and calcite respectively. The microstructural configuration of the sample after reaction shows grains of quartz, carbonates, pyrite surrounded by clay minerals. However, the pyrite grains and framboids show corrosion on their surfaces with dark patches as shown in Fig. 3b . The EDS weight % for Fe is observed to significantly reduce on the surface of pyrite grains which indicate reactions. The concentration of elements especially Ca on the EDS maps is also observed to be redistributed on the sample surface (Fig. 4b). This may be due to precipitation of amorphous phases, especially the Ca-rich amorphous phases on the sample surface. These phases tend to be deposited on fracture and pores spaces. From the SEM images, grain sizes and grain contacts do not show substantial difference from pre-experiment sample.

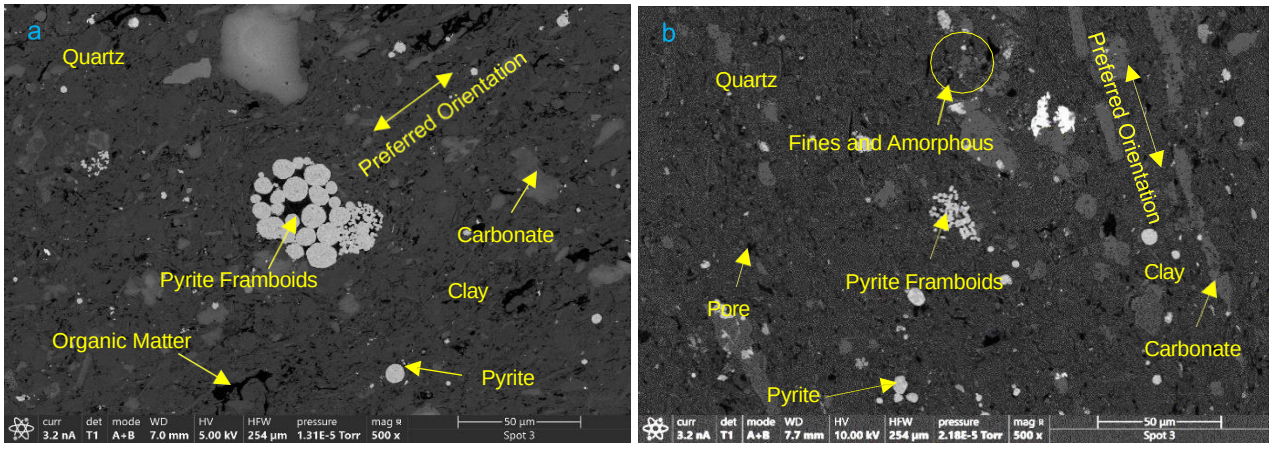

Fig. 3: SEM micrographs showing the mineralogy and microstructural configuration of Ductile sample cored parallel to the bedding plane. Clay minerals form a matrix with quartz, carbonate and feldspar grains completely embedded within the clay matrix. Preferred orientation is observed within the microstructure. a. sample before reaction showing substantial pore spaces; b. sample after reaction where pore spaces are filled with fines and amorphous entities.

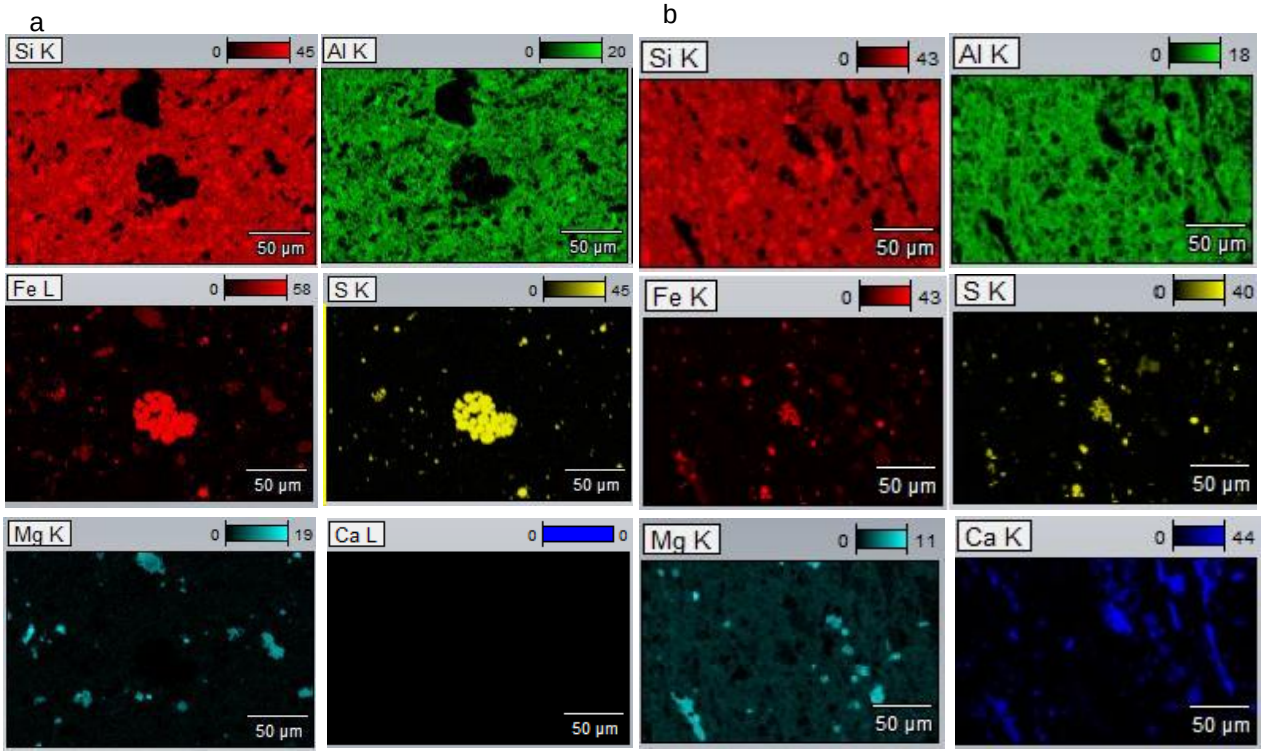

Fig. 4: EDS elemental maps (a and b) of the same areas on SEM micrographs showing the elemental concentrations and distributions on ductile (horizontal) sample before reaction (a. left) and after reaction (b. right) with produced brines. The presence of minerals phases in SEM micrographs are confirmed based on the elemental concentrations on the EDS maps.

3.2.2 Ductile Vertical Sample

The direction of coring is along the main core/wellbore axis (i.e perpendicular to the bedding plane). The microstructural configuration of the pre-reaction sample shows grains of quartz, carbonates, framboidal pyrite and disseminated pyrite surrounded by clay minerals as shown in Fig. 5a. The grain sizes most common in these samples range from 5µm to 30µm with an average grain size of less than 20µm. The common contact in the sample is grain-matrix contact, where the matrix is made of clay minerals. The sample also has significant pore and organic matter compositions as shown on Fig. 5a. Preferred orientation of minerals is not observed in this sample. In the post-reaction sample, the pyrite grains and framboids have dark spots on their surfaces, an indication of dissolution. The SEM also shows an increase in amorphous deposits on the surface of the sample as shown in Fig. 6b. The grain sizes and grain contacts however do not show substantial difference from pre-experiment sample. The EDS microanalysis shows presence of Si, Al, Mg, Fe, S, and Ca as elemental concentrations by weight % as observed in Fig. 6a and Fig. 6b. These elemental concentrations help to determine the mineralogy present in the sample as shown in Fig. 5a and Fig. 5b. The minerals identified include quartz, illite-smectite, dolomite, pyrite, plagioclase, and organic matter respectively.

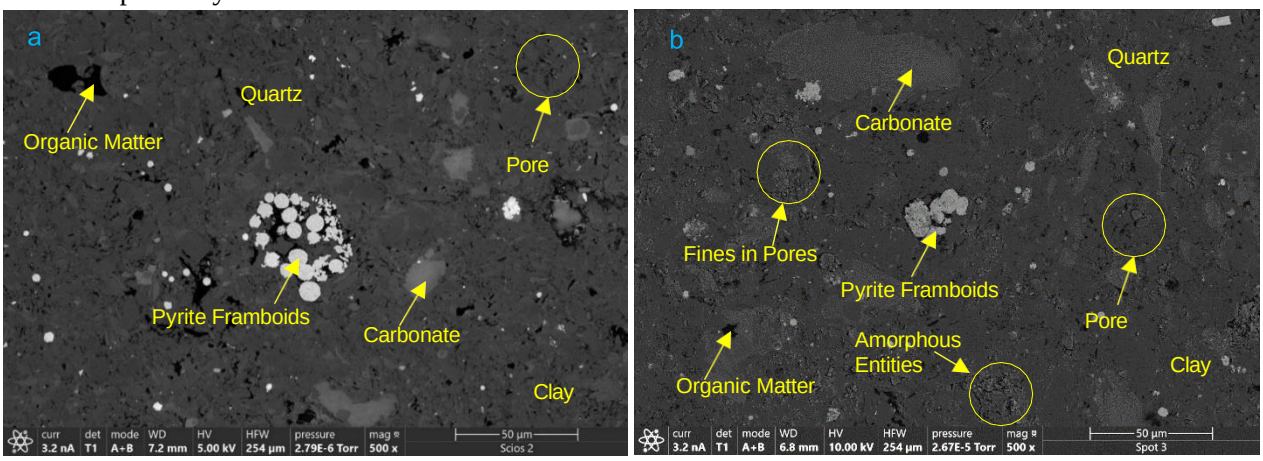

Fig. 5: SEM micrographs showing the mineralogy and microstructural configuration of Ductile sample cored perpendicular to the bedding plane. Clay minerals form a matrix with quartz, carbonate and feldspar grains completely embedded within the clay matrix. a. before reaction sample shows a substantial presence of pores and organic matter; b. after reaction sample where fine minerals and amorphous entities have been deposited in pores.

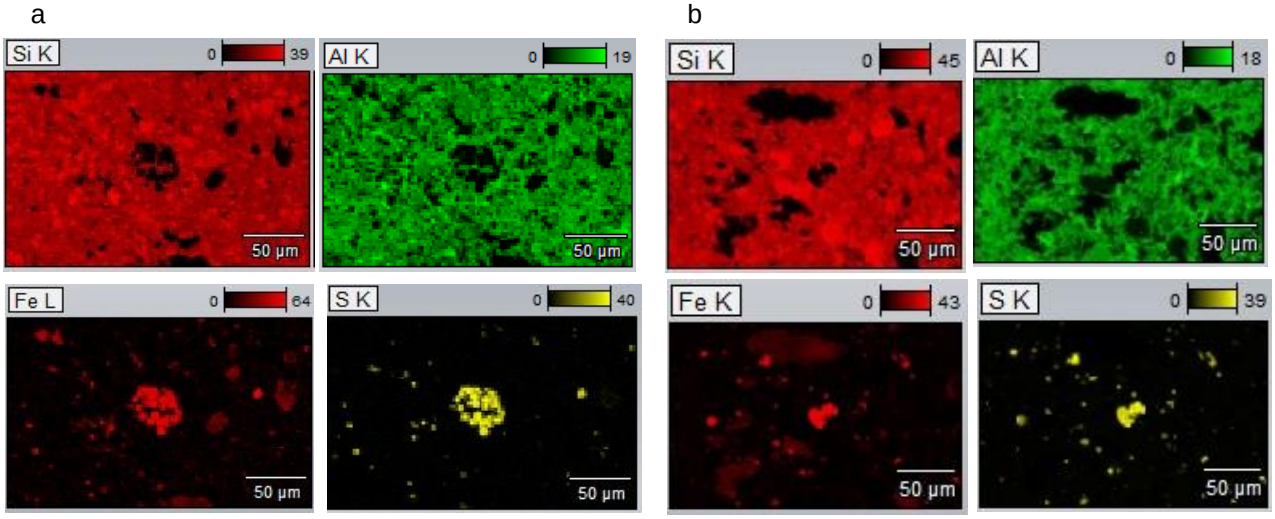

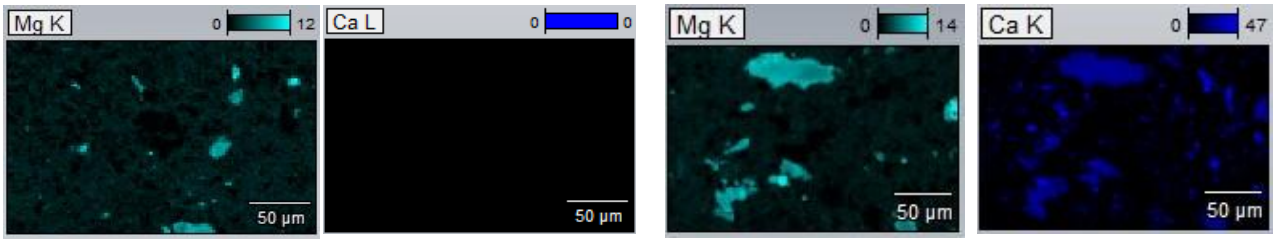

Fig. 6: EDS elemental maps (a and b) of the same area on SEM micrographs showing the elemental concentrations and distributions on ductile (vertical) sample before reaction (a. left) and after reaction (b. right) with produced brines. The presence of minerals phases in SEM micrographs are confirmed based on the elemental concentrations on the EDS maps.

3.2.3 Reservoir Horizontal Sample

The direction of coring is normal to the main core/wellbore axis (parallel to the bedding plane). The microstructural configuration of the sample before reaction shows grains of quartz, carbonates, feldspars, and pyrite (large grains, framboidal and disseminated) in matrix of clay minerals and carbonate cements. The sample shows significant pore volume along the grain contacts. The common contact in the sample is grain-grain contact relative to the grain to matrix contacts observed in the ductile samples. The grain sizes most common in these samples range from 15µm to 40µm with an average grain size of approximately 35µm shown in Fig. 7a. Preferred orientation of minerals is generally absent in this sample though it was cored along the bedding plane of the sample. The microstructural configuration of the sample after reaction does not show substantial changes from SEM images. In terms of mineralogy, pyrite dissolution is evident from SEM images in Fig. 7b. The grains and framboids of pyrite show dark spots on their surfaces which were previously bright, an indication of reduced concentrations of iron. Carbonate halos are also observed on some mineral grains, mostly quartz and feldspars (dark grains). This may be a result of mineral reaction and transformation due to the high calcium concentrations in produced brines. Si, Al, Mg, Fe, S, and Ca elements are observed in EDS mapping and recorded in weight % presented in Fig. 8a and Fig. 8b. These elemental concentrations correspond to quartz, illite-smectite, dolomite, pyrite, plagioclase, and calcite in Fig. 7a and Fig. 7b respectively.

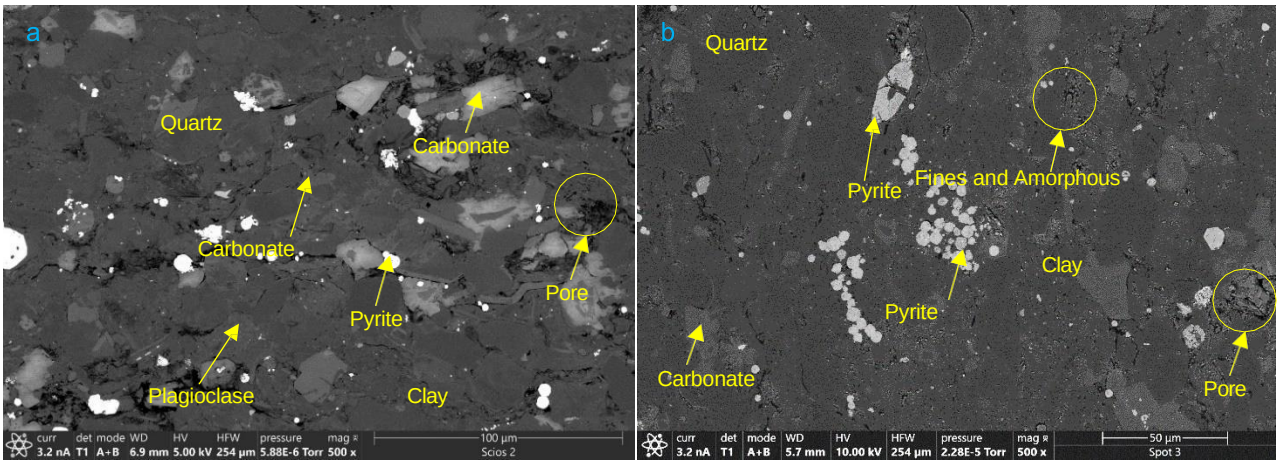

Fig. 7: SEM micrographs showing the mineralogy and microstructural configuration of reservoir sample cored parallel to the bedding plane. The sample is characterized by bigger grains with significant grain-to-grain contacts. a. sample before reaction shows significant pore spaces along the grain contacts; b. sample after reaction where most of the pores are filled with fine minerals and amorphous entities.

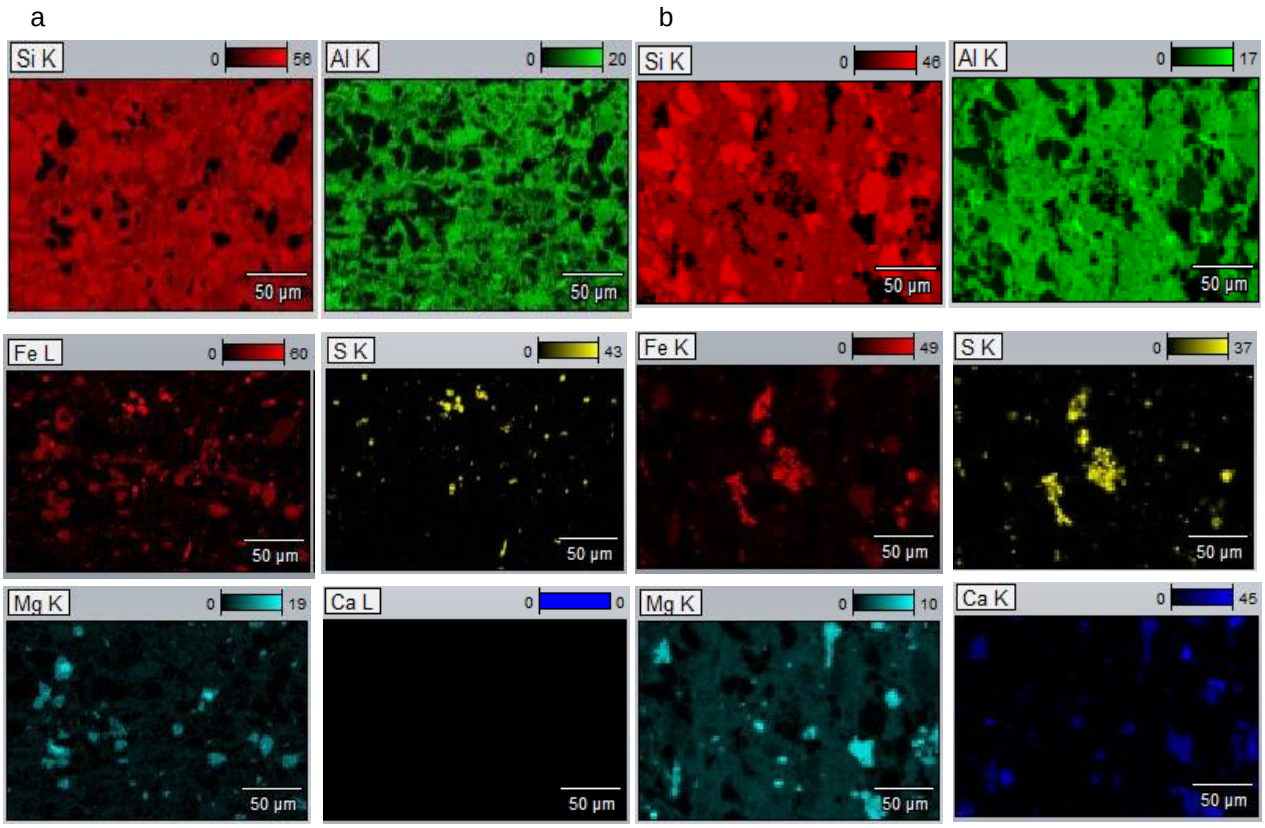

Fig. 8: EDS elemental maps (a and b) of the same area on SEM micrographs showing the elemental concentrations and distributions on reservoir (horizontal) sample before reaction (a. left) and after reaction (b. right) with produced brines. The presence of minerals phases in SEM micrographs are confirmed based on the elemental concentrations on the EDS maps.

3.2.4 Reservoir Vertical Sample

The direction of coring is parallel to the main core/wellbore axis (i.e perpendicular to the bedding plane). The microstructural configuration of the sample shows grains of quartz, carbonates, feldspars, and pyrite (large grains, framboidal and disseminated) in matrix of clay minerals and carbonate cements. The common contact in the sample is grain-to-grain contact with significant pore volume along these contacts as observed in Fig. 9a. The grain sizes most common in these samples range from 10µm to 40µm with an average grain size of approximately 35µm. Preferred orientation of minerals is generally absent in this sample. The microstructural configuration of the sample after reaction does not show substantial changes from SEM images. In terms of mineralogy, the preponderance of amorphous entities on the surface of the sample as well as pyrite dissolution is evident from SEM images in Fig. 9b. Some mineral grains, mostly quartz and feldspars (dark grains) show high carbonate compositions forming halos around them. This is an indication of mineral reaction and transformation due to the high calcium concentrations in produced brines. The EDS microanalysis shows the presence of Si, Al, Mg, Fe, S, and Ca in different elemental concentrations by weight % shown in Fig. 10a and Fig. 10b. These elemental concentrations help to determine the minerals as shown in Fig. 9a and Fig. 9b respectively. The minerals identified include quartz, illite-smectite, dolomite, pyrite, plagioclase, and K-feldspar.

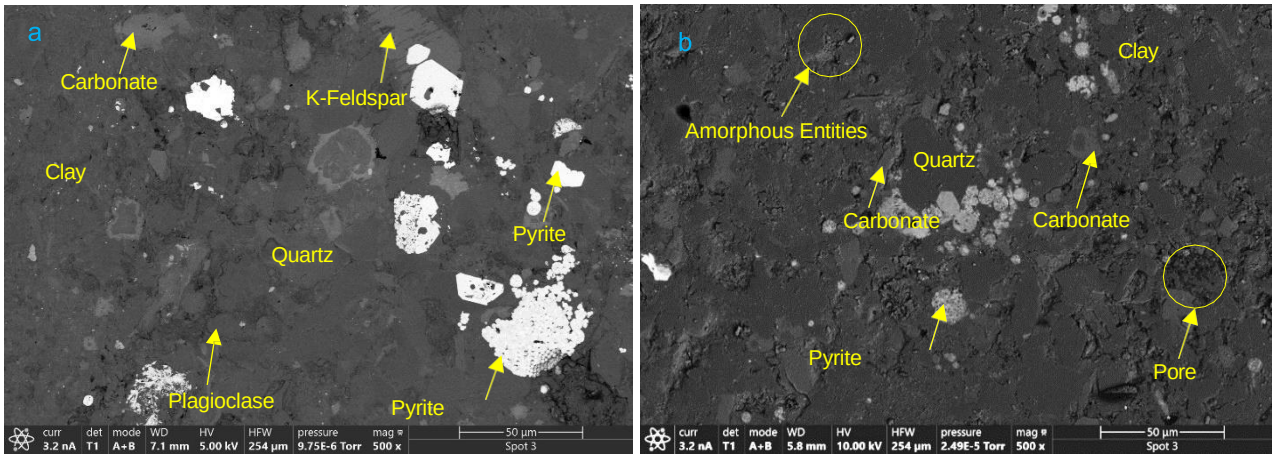

Fig. 9: SEM micrographs showing the mineralogy and microstructural configuration of reservoir sample cored normal to the bedding plane. The sample is characterized by bigger grains with grain-to-grain contacts being common. a. sample before reaction shows significant pore spaces along the grain contacts; b. sample after reaction where most of the pores are filled with fine minerals and amorphous entities.

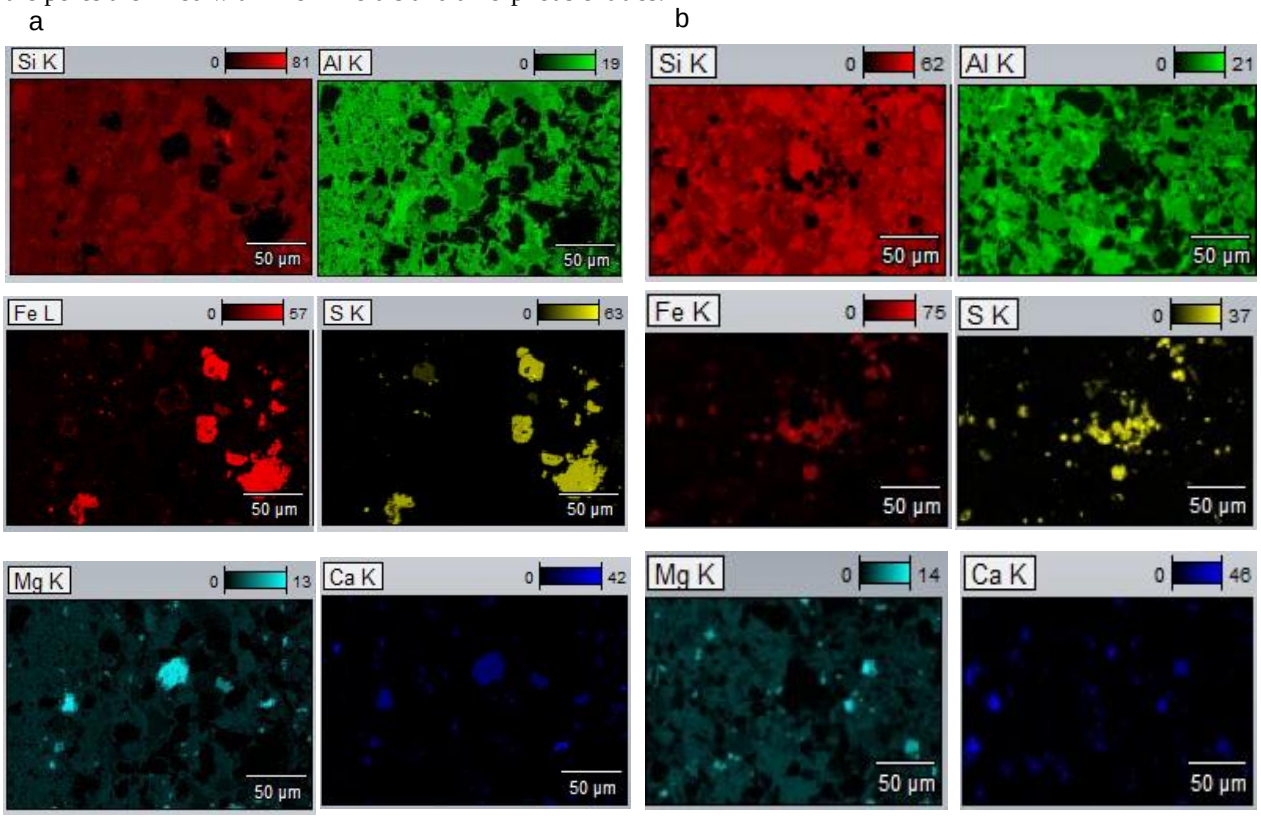

Fig. 10: EDS elemental maps (a and b) of the same area on SEM micrographs showing the elemental concentrations and distributions on reservoir (vertical) sample before reaction (a. left) and after reaction (b. right) with produced brines. The presence of minerals phases in SEM micrographs are confirmed based on the elemental concentrations on the EDS maps.

3.4 Significance of Microstructure

SEM micrographs combined with EDS microanalysis provide an avenue to understand the mineral distribution within rocks and consequently the microstructure of the rocks. From the results, it is observed that significant disparities exist between various samples – pre-experiment versus post-experiment, reservoir versus ductile and horizontal versus vertical. These determine the response to fracturing within the various formations and the mechanisms that affect their conductivity.

The samples used in the experiments stated above represent ductile and reservoir zones of the Caney Shale. In the ductile zone, the high clay content encapsulating smaller grains of quartz, carbonates and feldspars induce ductile properties in the rock. Ductility is associated with high clay content in rocks, due to the ability of these minerals to undergo significant elastic strains. Therefore, during hydraulic fracturing, the energy applied to create fractures is absorbed by the clay minerals mostly through high elastic strain with low plastic strain. In case fractures are created in this type of rock unit, later stage deflocculation of clay minerals provides sufficient fines to cause the occlusion and closure of these fractures. In contrast, the reservoir zone is characterized by bigger grains of quartz, carbonate, and feldspar minerals within clay matrix. This sample has a higher frequency of grain-to-grain contact which leads to higher brittleness relative to ductile sample. During hydraulic fracturing, the stress exerted causes significant plastic strain and thus creates sufficient number of fractures to substantially increase the permeability of the formation. From the foregoing, the importance of microstructural configuration of a formation is inherently important to the fracability of the formation.

3.5 Comparison to Past Studies

The established protocol of hydraulic fracturing in unconventional shale reservoirs involves the shut-in of wells for one to several weeks after completion of the injection process (Bertoncello et al., 2014; Jew et al., 2022; Speight, 2016). During this period, fluids are imbibed into fracture walls which trigger complex reactions that may be detrimental to reservoir permeability. This necessitated several studies to understand the geochemical rock-fluid reaction with shales. Two of these studies that are closer to the current study are compared to aid in appreciating the observations from the current study.

Dieterich et al., (2016), studied the rock-fluid reaction between Huntersville Chert in Pennsylvania and recycled fluids from the field, mainly using the Field Emission Scanning Electron Microscope (FE-SEM). They conducted these experiments at temperature and pressure of 50^{o}C and 1500 psi respectively for 89 days. They reported the precipitation of barite, celestite, strontianite and apatite on the surface of reacted samples which are associated with barium, sulfate, and carbonate ions. In this study, no evidence of carbonate dissolution was observed but the increase in pH from 4.3 to 6.2 may have been the result of carbonate dissolution. In the current experiment, the surface of post- reacted rock-slab shows precipitated minerals and amorphous entities with high Ca concentrations. The concentrations of Fe, Na, Al and Si are also high within the amorphous entities, which indicate newly precipitated material on the rock surface. The results from XRD analysis of rock powders however show dissolution of pyrite, feldspar and illite which are synonymous with elemental concentrations of Fe, Na, Al, and Si. There is however minimal carbonate (calcite and dolomite) dissolution.

Jew et al., (2017) conducted experiments on Marcellus, Barnett, Eagle Ford, and Green River Formations to understand the contribution of Fe (II) oxidation to permeability loss. These experiments were conducted at 80^{o}C using whole-rock chips and sand-size particles in fracturing fluids containing hydrochloric acid and fracturing fluid without hydrochloric acid. Results showed that initial pH of fracturing fluid was the most important factor in the release of Fe into solution. In reaction with low pH (2.0) solutions, sand sized samples with low carbonate compositions released significant Fe into solution within a short period, which was followed by short periods of plateau and a sharp drop in iron concentration in solution. The drop in iron concentration was defined as a period of iron-based mineral precipitation. In contrast, sand-sized samples with high carbonate composition witnessed low to no release of iron into solution. Also, in reactions with no hydrochloric acid added to fracturing fluid, there was no release of iron into solution. Reactions between low pH fluid and carbonate-poor whole-rock samples showed slower rates of Fe release and slower rates of iron mineral precipitation compared to sand sized samples. In the current

study, produced fluids are not acidized but the rock-slab is considered an equivalent of the whole-rock whilst powders are the equivalent of the sand-size rocks. The concentration of Fe in pyrite grains on the rock-slab surface is observed to significantly reduce after reaction (shown by dark spots on SEM images and reduced Fe elemental weight % on EDS maps). These are redistributed and precipitated in minerals and amorphous entities throughout the sample surface. The XRD analysis confirms the dissolution of pyrite which will lead to increased concentrations of Fe(II) in solution thus may cause precipitation. The conclusion from these observations, as with Jew et al. (2017), is that the breakdown of pyrite, followed by the oxidation and redistribution of Fe can lead to plugging of fractures and thus rapid permeability decline.

4.0 Conclusions

Hydraulic fracturing remains the most widespread mode of tight reservoir stimulation to enhance permeability for exploiting hydrocarbons from shales with ultra-low permeability. However, the heterogeneity of these reservoirs and the complexity inherent in clay matrix and other minerals in these formations make sustainability of the generated permeability challenging. Based on the results and discussions of rock-fluid reactions in the Caney Shale above, the following conclusions are made.

- There is high potential for long-term post-fracturing geochemical reactions in the Caney Shale with adverse impact on permeability of fractures and consequently productivity.
- Breakdown of pyrite occurs rapidly after exposure to brine. This can lead to generation of acids which reduces the pH of fluids temporarily, thus catalyzing breakdown of other minerals especially carbonates and feldspars.
- High concentration of elements in injected brine causes the precipitation of minerals and formation of amorphous entities that can plug fractures and other hydrocarbon flow paths to cause significant permeability decline.
- Amorphous entities on the surface of rock slabs had high concentration of elements associated with clay minerals giving an indication that these entities originate from the breakdown of clay minerals. This shows the instability of clay minerals which can breakdown to generate fines. These fines can cause substantial formation damage and jeopardize the long-term permeability of hydraulically fractured shale reservoirs.
- Analysis of post-reaction fluid compositions is planned for the next phase of this study. This will help to attain complete appreciation of reaction trends during shale rock interaction with produced fluid.

Acknowledgements

The authors of this paper would like to acknowledge this study was sponsored by DOE Award DE-FE0031776 from the Office of Fossil Energy. Many thanks to our industry partners for their immense support in providing rock and fluid samples for this work. The authors are grateful to Lisa Whitworth and Brent Johnson at the OSU Venture 1 Microscopy Facility for their support during data acquisition. Finally, the authors also wish to thank our colleagues in Barrier Material and Geomimicry Laboratory, Ben Anderson, Loic Bethel Dje and Paschalyn Edem Nyavor for their support.

References

Aftab, A., Ali, M., Sahito, M. F., Mohanty, U. S., Jha, N. K., Akhondzadeh, H., Azhar, M. R., Ismail, A. R., Keshavarz, A., and Iglauer, S. 2020. Environmental friendliness and high performance of multifunctional tween 80/ZnO-nanoparticles-added water-based drilling fluid: an experimental approach. *ACS Sustainable Chemistry and Engineering*, *8*(30), 11224–11243.

Ahmed, A., Alsaihati, A., and Elkatatny, S. 2021. An overview of the common water-based formulations used for drilling onshore gas wells in the Middle East. *Arabian Journal for Science and Engineering*, *46*(7), 6867–6877.

Allen, C., Katende, A., Xiong, F., Massion, C., Krumm, R., and Radonjic, M. 2022. Subsurface Engineering of Conductive Fractures in Caney Shale, Southern Oklahoma: A Step Towards Energy Transition. *2022 Goldschmidt Conference*.

Almulhim, A., Alharthy, N., Tutuncu, A. N., and Kazemi, H. 2014. Impact of imbibition mechanism on flowback behavior: a numerical study. *Abu Dhabi International Petroleum Exhibition and Conference*.

Awejori, G. A., Doughty, C., Xiong, F., Paronish, T., Spycher, N., and Radonjic, M. 2022. Integrated Experimental and Modeling Study of Geochemical Reactions of Simple Fracturing Fluids with Caney Shale. *Energy & Fuels*, *36*(17), 10064–10081.

Awejori, G. A., Luo, G., Grider, C., Katende, A., Radonjic, M., Doughty, C., Spycher, N., Paronish, T., O'Connell, L., and Rihn, A. 2021. Fracturing Fluid-Induced Mineralogy Changes and Impact on Elastic Properties for the Caney Shale, Oklahoma. *55th US Rock Mechanics/Geomechanics Symposium*.

Awejori, G., Xiong, F., Katende, A., Radonjic, M., Whitworth, L., and Paronish, T. 2022. Fluid Induced Elemental and Mineralogy Alterations of Caney Shale. *ARMA US Rock Mechanics/Geomechanics Symposium*, ARMA-2022.

Benge, M., Lu, Y., Katende, A., Rutqvist, J., Crandall, D., Haecker, A., King, G., Renk, J. B., Radonjic, M., and Bunger, A. 2021. Connecting geomechanical properties with potential for proppant embedment and production decline for the emerging caney shale, oklahoma. *SPE/AAPG/SEG Unconventional Resources Technology Conference*, D011S002R001.

Bertoncello, A., Wallace, J., Blyton, C., Honarpour, M., and Kabir, C. S. S. 2014. Imbibition and water blockage in unconventional reservoirs: well-management implications during flowback and early production. *SPE Reservoir Evaluation and Engineering*, *17*(04), 497–506.

Chakraborty, N., Karpyn, Z. T., Liu, S., and Yoon, H. 2017. Permeability evolution of shale during spontaneous imbibition. *Journal of Natural Gas Science and Engineering*, *38*, 590–596.

Dewhurst, D. N., Jones, R. M., and Raven, M. D. 2002. Microstructural and petrophysical characterization of Muderong Shale: application to top seal risking. *Petroleum Geoscience*, *8*(4), 371–383.

Dieterich, M., Kutchko, B., and Goodman, A. 2016. Characterization of Marcellus Shale and Huntersville Chert before and after exposure to hydraulic fracturing fluid via feature relocation using field-emission scanning electron microscopy. *Fuel*, *182*, 227–235.

Downey, M. W. 1984. Evaluating seals for hydrocarbon accumulations. *AAPG Bulletin*, *68*(11), 1752–1763.

Esteves, B. F., Spielman-Sun, E., Li, Q., Jew, A. D., Bargar, J. R., and Druhan, J. L. 2022. Geochemical Modeling of Celestite (SrSO4) Precipitation and Reactive Transport in Shales. *Environmental Science and Technology*, *56*(7), 4336–4344.

Feng, Y., Xiao, X., Wang, E., Sun, J., and Gao, P. 2021. Oil retention in shales: A review of the mechanism, controls and assessment. *Frontiers in Earth Science*, *9*, 720839.

Fu, X., Cueto-Felgueroso, L., Bolster, D., and Juanes, R. 2015. Rock dissolution patterns and geochemical shutdown of–brine–carbonate reactions during convective mixing in porous media. *Journal of Fluid Mechanics*, *764*, 296–315.

Harrison, A. L., Jew, A. D., Dustin, M. K., Thomas, D. L., Joe-Wong, C. M., Bargar, J. R., Johnson, N., Brown, G. E., and Maher, K. 2017. Element Release and Reaction-Induced Porosity Alteration during Shale-Hydraulic Fracturing Fluid Interactions. *Appl. Geochem.*, *82*, 47.

Jew, A. D., Druhan, J. L., Ihme, M., Kovscek, A. R., Battiato, I., Kaszuba, J. P., Bargar, J. R., and Brown Jr, G. E. 2022. Chemical and Reactive Transport Processes Associated with Hydraulic Fracturing of Unconventional Oil/Gas Shales. *Chemical Reviews*, *122*(9), 9198–9263.

Jew, A. D., Dustin, M. K., Harrison, A. L., Joe-Wong, C. M., Thomas, D. L., Maher, K., Brown Jr, G. E., and Bargar, J. R. 2017. Impact of organics and carbonates on the oxidation and precipitation of iron during hydraulic fracturing of shale. *Energy and Fuels*, *31*(4), 3643–3658.

Katende, A., Allen, C., Rutqvist, J., Nakagawa, S., and Radonjic, M. 2023. Experimental and numerical investigation of proppant embedment and conductivity reduction within a fracture in the Caney Shale, Southern Oklahoma, USA. *Fuel*, *341*, 127571.

Khosrokhavar, R., Griffiths, S., and Wolf, K.-H. 2014. Shale gas formations and their potential for carbon storage: opportunities and outlook. *Environmental Processes*, *1*, 595–611.

Li, Q., Jew, A. D., Brown Jr, G. E., Bargar, J. R., and Maher, K. 2020. Reactive transport modeling of shale–fluid interactions after imbibition of fracturing fluids. *Energy and Fuels*, *34*(5), 5511–5523.

Liu, S., Wang, J., He, H., and Wang, H. 2018. Mechanism on imbibition of fracturing fluid in nanopore. *Nanoscience and Nanotechnology Letters*, *10*(1), 87–93.

Luning, S., Shahin, Y. M., Loydell, D., Al-Rabi, H. T., Masri, A., Tarawneh, B., and Kolonic, S. 2005. Anatomy of a world-class source rock: Distribution and depositional model of Silurian organic-rich shales in Jordan and implications for hydrocarbon potential. *AAPG Bulletin*, *89*(10), 1397–1427.

Maiti, M., Bhaumik, A. K., and Mandal, A. 2021. Performance of water-based drilling fluids for deepwater and hydrate reservoirs: Designing and modelling studies. *Petroleum Science*, *18*(6), 1709–1728.

Marcon, V., Joseph, C., Carter, K. E., Hedges, S. W., Lopano, C. L., Guthrie, G. D., and Hakala, J. A. 2017. Experimental insights into geochemical changes in hydraulically fractured Marcellus Shale. *Applied Geochemistry*, *76*, 36–50.

Morse, J. W., and Arvidson, R. S. 2002. The dissolution kinetics of major sedimentary carbonate minerals. *Earth-Science Reviews*, *58*(1–2), 51–84.

Mukhina, E., Cheremisin, A., Khakimova, L., Garipova, A., Dvoretskaya, E., Zvada, M., Kalacheva, D., Prochukhan, K., Kasyanenko, A., and Cheremisin, A. 2021. Enhanced oil recovery method selection for shale oil based on numerical simulations. *ACS Omega*, *6*(37), 23731–23741.

Olabode, A., and Radonjic, M. 2017. Fracture conductivity modelling in experimental shale rock interactions with aqueous CO2. *Energy Procedia*, *114*, 4494–4507.

Shaw, D. B., and Weaver, C. E. 1965. The mineralogical composition of shales. *Journal of Sedimentary Research*, *35*(1), 213–222.

Soeder, D. J. 2018. The successful development of gas and oil resources from shales in North America. *Journal of Petroleum Science and Engineering*, *163*, 399–420.

Speight, J. G. 2016. *Handbook of hydraulic fracturing*. John Wiley & Sons.

Tayari, F., Blumsack, S., Dilmore, R., and Mohaghegh, S. D. 2015. Techno-economic assessment of industrial CO2 storage in depleted shale gas reservoirs. *Journal of Unconventional Oil and Gas Resources*, *11*, 82–94.

Wang, Y., Luo, G., Achang, M., Cains, J., Wethington, C., Katende, A., Grammer, G. M., Puckette, J., Pashin, J., and Castagna, M. 2021. Multiscale characterization of the caney shale—an emerging play in Oklahoma. *Midcontinent Geoscience*, *2*, 33–53.

Wood, T., and Milne, B. 2011. Waterflood potential could unlock billions of barrels: Crescent Point Energy. In *2013-05-20]. http://www. investorvillage. com/uploads/44821/files/CPG dundee. pdf*.

Xiong, F., Rother, G., and Radonjic, M. 2022. Insights into Controls of Mineralogy and Pore Structure on the Density of Methane Adsorption Phase in Shales under Supercritical Conditions. *Energy and Fuels*, *36*(17), 10110–10122.

Yalman, E., Federer-Kovacs, G., Depci, T., Al Khalaf, H., Aylikci, V., and Aydin, M. G. 2022. Development of novel inhibitive water-based drilling muds for oil and gas field applications. *Journal of Petroleum Science and Engineering*, *210*, 109907.

Zhou, Z., Abass, H., Li, X., Bearinger, D., and Frank, W. 2016. Mechanisms of imbibition during hydraulic fracturing in shale formations. *Journal of Petroleum Science and Engineering*, *141*, 125–132.